Bull. Fish. Sci. Hokkaido Univ.
55(1), 35-42, 2004.

Formation and Structure of the Barotropic Flow over the Shallow Shelf Slope Region

Yutaka ISODA

(Received 17 February 2004, Accepted 26 May 2004)

Abstract

The formation and structure of the steady barotoropic flow over the shallow shelf slope are investigated using the theory with linear bottom friction and the numerical experiments with quadratic bottom friction. The barotropic flow over the shallow shelf slope, which is controlled by the bottom friction, has the balance between bottom stress curl and vortex stretching of water column. Such flow cannot conserve its volume transport to the downstream due to the onshore or offshore flow. The formation of barotoropic flow is related with the coastal-trapped wave propagation, i.e., Kelvin wave or topographic Rossby wave, during the transient period like as the geostropic adjustment. Therefore, the steady barotropic flow is formed in the direction of wave propagation, i.e., at the right hand sidewall to the source of disturbance in the northern hemisphere. By using the numerical model in which the ideal topography around the Tsushima/Korea Strait is taken into account and the flow system is driven by the sea level difference between the East China Sea and the Japan Sea, the flow patterns in winter are considered. In result, two branches in the central part of the East China Sea can be simulated. One northward branch is clockwise-flow along the isobaths in the northern part of the East China Sea and the other eastward branch directly inflows into the Tsushima/Korea Strait.

Key words: barotoropic flow, shallow shelf slope, bottom friction

Introduction

The Tsushima/Korea Strait is situated between the East China Sea and the Japan Sea shown in Fig. 1. The Tsushima Current flows into the Japan Sea through the Tsushima/Korea Strait due to the sea level difference between both areas. The East China Sea and the Tsushima/Korea Strait are very shallow with a maximum depth about 100 m, and their density structure is a homogeneous vertically in wintertime due to the vertical mixing associated with the winter cooling. However, the detail flow structure in this area has not observed still now.

Yoon(1982) and Kawabe(1982) investigated the formation mechanisms of flow on the shelf slope with use of the numerical model, and showed that the flow on the shelf is the bottom controlled steady flow due to the topographic-β effect. In the real situation, over the shallow shelf slope region like as the East China Sea and the Tsushima/Korea Strait, the bottom friction must play an essential role in such flow. In the present study, the barotropic flow structure over the shallow shelf slope will be analyzed theoretically taking into account of the liner bottom friction, and the formation mechanism of such flow will be examined by using the numerical model. Then, we will investigate the brotropic flow around the Tsushima/Korea Strait in winter.

Analytical solution

We chose a right-handed coordinate system, so that the x-axis coincides with the coast, positive y pointing offshore, as shown in Fig. 2. We suppose that the depth is only a function of offshore distance y, and that the constant shelf slope region is confined to a near-shore band of width W. The driving force is the alongshore component of the inflow, i.e., $u(0, y)$, at the left end of the shelf slope region.

We consider the steady state problem with a linear bottom friction. The dynamical equations for the depth-averaged velocities are

$$-fv=-g\frac{\partial \eta}{\partial x}-\frac{ru}{h} \tag{1}$$

$$fu=-g\frac{\partial \eta}{\partial y} \tag{2}$$

$$h\left(\frac{\partial u}{\partial x}+\frac{\partial v}{\partial y}\right)+v\frac{dh}{dy}=0 \tag{3}$$

Laboratory of Marine Environmental Science, Graduate School of Fisheries Sciences, Hokkaido University
(e-mail: isoda@sola3.fish.hokudai.ac.jp)
(北海道大学大学院水産科学研究科資源環境科学講座)

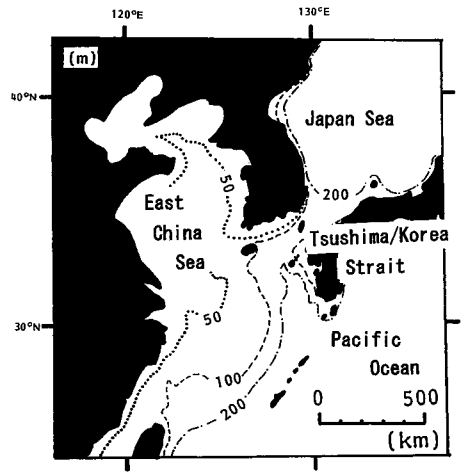

Fig. 1 The bottom topography around the Tsushima/Korea Strait.

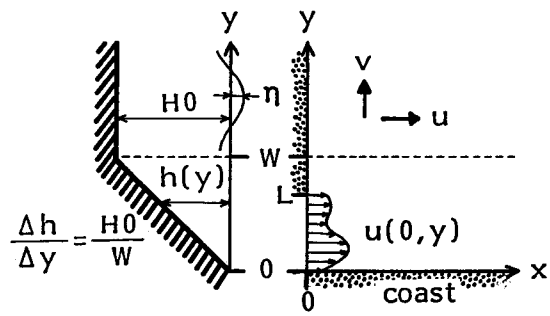

Fig. 2 The topographic configuration and coordinate system of the model.

where u and v are depth-averaged components of velocity in x- and y-directions, respectively; η is the elevation of sea surface; r is a bottom resistance coefficient with the dimension of velocity; g is the acceleration due to gravity; $h=h(y)$ is the depth; f is the Coriolis parameter. At the first approximation, the barotropic flow over the shelf slope flows along the isobaths due to the conservation of the potential vorticity, i.e., $f/h(y)$ is conserved. Therefore, the alongshore flow is dominant compared to the offshore flow over the shelf. That is, equation (2) is valid only if

$$|fu| \gg \left|\frac{rv}{h}\right| \qquad (4).$$

Such a problem has some similarities to the work of Csanady (1978), which studied the arrested topographic wave generated by the alongshore wind component.

Elimination of η from equations (1) and (2) and using of equation (3) lead to the vorticity equation;

$$\frac{\partial}{\partial y}\left(\frac{ru}{h}\right)+\frac{f}{h}\frac{dh}{dy}v=0 \qquad (5).$$

The first term of equation (5) is the curl of bottom stress, which is balanced by the vortex stretching term. Here, when v assumes to be zero, the offshore distributions of u may be computed use of equation (5), i.e., $u(y)\propto h(y)$, but such distribution of alongshore velocity u should be unrealistic. On the general shelf slope, if $u>0$ and $u\to 0$ at $y\to\infty$, the bottom stress curl: $\frac{\partial}{\partial y}\left(\frac{ru}{h}\right)=\frac{1}{h}\frac{\partial u}{\partial y}-\frac{u}{h}\frac{dh}{dy}$ becomes negative at least near the offshore shelf area because of $\frac{1}{h}\frac{\partial u}{\partial y}<0$ and $\frac{u}{h}\frac{dh}{dy}>0$. This implies that the velocity v over the shelf slope is positive. That is, the alongshore steady-state barotropic flow ($u>0$) must be maintained by the offshore transport ($v>0$). Thus, such flow over the shelf slope cannot conserve its volume transport to the downstream.

Eliminating u and v from equations (1), (2) and (3), an equation for the surface elevation is as follows;

$$\frac{\partial \eta}{\partial x}=k^2\frac{\partial^2 \eta}{\partial y^2} \qquad (6)$$

where

$$k^2=\left(\frac{f}{r}\frac{dh}{dy}\right)^{-1} \qquad (7).$$

Equation (6) has the form of heat conduction equation with positive x playing the role of time, when k^2 assumes to be thermometric conductivity. Equation (6) will be solved with the following boundary conditions.

(i) The boundary condition along the coast is that the normal flow vanishes, i.e., $v(x,0)=0$. From equations (2) at $y=0$, we have

$$\frac{\partial \eta}{\partial y}=0 \text{ at } y=0 \qquad (8).$$

(ii) As $dh/dy=0$ beyond $y=W$, equation (6) shows $\frac{\partial^2 \eta}{\partial y^2}=0$ or $\frac{\partial \eta}{\partial y}=$constant ($y>W$). Suppose that the offshore gradient of surface elevation vanishes at $y\to\infty$, we have the boundary condition at the shelf edge of $y=W$ as follows;

$$\frac{\partial \eta}{\partial y}=0 \text{ at } y=W \qquad (9).$$

(iii) The driving force at $x=0$ is assumed as the alongshore flow with offshore width L. Then, using equation (2),

$$\eta(0,y)=-\frac{f}{g}\int_0^y u(0,y)dy=\phi(y) \qquad (10).$$

With the method of a separation of variable, the solution $\eta(x,y)$ is assumed as follows,

$$\eta(x,y)=X(x)Y(y) \qquad (11).$$

Substituting equation (11) into equation (6), we have following two equations,

$$Y''+(\lambda/k)^2 Y=0 \qquad (12)$$

$$X'+\lambda^2 X=0 \qquad (13)$$

where the prime denotes differentiation with respect to y for equation (12) and x for equation (13), and λ is the positive coefficient. The general solution of equation (12) using the boundary conditions of (8) and (9) is

$$Y(y)=\cos\left(\frac{\lambda y}{k}\right) \qquad (14)$$

where λ is given by

$$\lambda=\frac{n\pi k}{W} \quad (n=1, 2, 3....) \qquad (15).$$

The general solution of equation (13) is

$$X(x)=e^{-\lambda^2 x} \qquad (16).$$

$\eta(x, y)$ is expanded using equations (14), (15) and (16) in the form

$$\eta(x, y)=\sum_{n=1}^{\infty} A_n \cdot \cos\left(\frac{n\pi y}{W}\right) \cdot e^{-\frac{n^2\pi^2 k^2}{W^2}x} \qquad (17)$$

where

$$A_n=\frac{2}{W}\int_0^W \phi(y)\ \cos\left(\frac{n\pi y}{W}\right)dy \qquad (18)$$

which can be obtained substituting the boundary condition of (10) into equation (18). From equations (1), (2) and (17), the velocity u and v may be expressed as follows;

$$u(x, y)=\frac{g}{f}\sum_{n=1}^{\infty} A_n \frac{n\pi}{W} \sin\left(\frac{n\pi y}{W}\right) e^{-\frac{n^2\pi^2 k^2}{W^2}x} \qquad (19)$$

$$v(x, y)= -\frac{rg}{f}\sum_{n=1}^{\infty} A_n \left\{\frac{n\pi}{H0}\cos\left(\frac{n\pi y}{W}\right)-\frac{1}{h}\sin\left(\frac{n\pi y}{W}\right)\frac{2\pi}{W}\right\} e^{-\frac{n^2\pi^2 k^2}{W^2}x} \qquad (20)$$

From these solutions, it may be seen that the fundamental flow, $n=1$, is only dominant at the far downstream and the maximum alongshore velocity u exists at the center of the shelf width, i.e., $y=W/2$.

We model the typical shelf bottom topography with linear slope around the Tsushima/Korea Strait and the driving inflow from the entrance at $x=0$. The following values are adopted ; W (shelf width)$=100$ km, $H0$ (depth of outer shelf region)$=100$ m, L (inflow entrance width)$=50$ km, r (resistance coefficient)$=0.04$ cm s^{-1}, f (Coriolis parameter)$=8.58\times10^{-5}$ s^{-1}. The alongshore velocity profile is assumed as follows;

$$u(0,y) = \begin{cases} 40\text{ cm s}^{-1} & \text{at } 0<y<L \\ 0\text{ cm s}^{-1} & \text{at } y>L \end{cases} \qquad (21).$$

This inflow volume transport is 1 Sv, which value is equivalent to that of the Tsushima Current in winter (Toba et al., 1982).

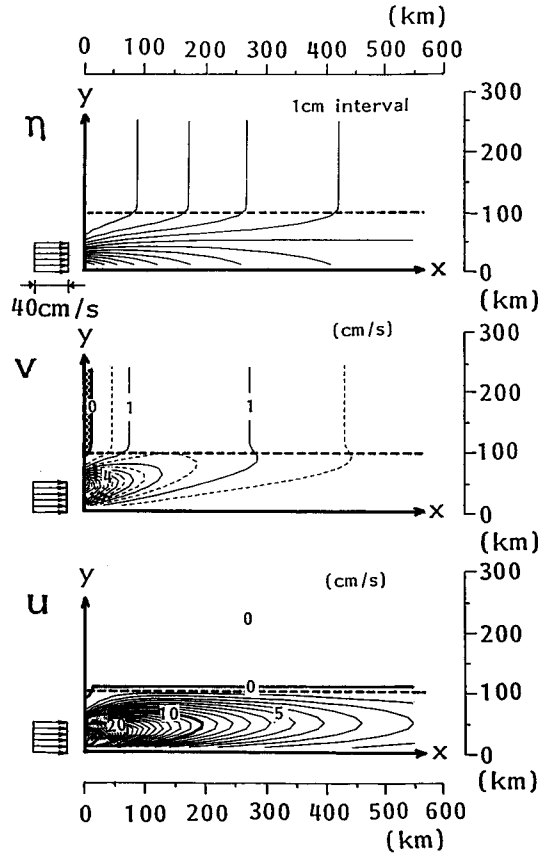

Fig. 3 Horizontal distributions of sea level η (top), offshore velocity v (middle) and alongshore velocity u (bottom) given by the theory. Thick broken line denotes the end of the shelf slope and the negative velocity region is shaded.

Figure 3 shows the spatial distribution of η, u and v for this case. As the distance from the entrance increases, the offshore gradient of η becomes smaller gradually. The alongshore flow u is confined to the shelf slope region, but its velocity tends to decrease in the same manner as the offshore gradient of η, because the offshore flow v is positive, which is larger especially near the entrance.

Numerical experiments

The previous section has shown that the steady barotropic flow over the shelf slope is formed under the balance between the bottom stress curl and the vortex stretching of water column due to the offshore flow. Now, we will consider the formation mechanism of such barotropic flow with use of the time-dependent numerical experiments.

Model

We consider a homogeneous ocean shown in Fig. 4.

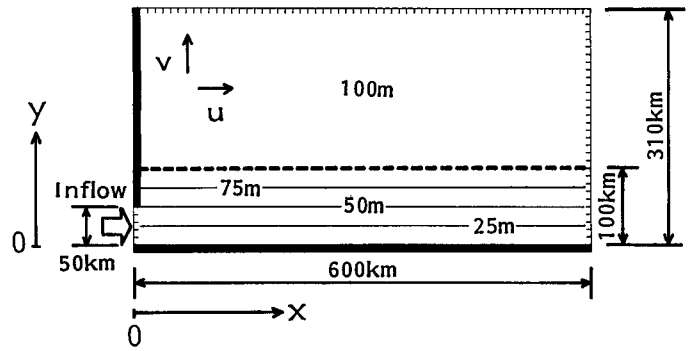

Fig. 4 Schematic view of the model ocean used in the numerical study.

The alongshore length of the model ocean is 600km and the offshore length is 310 km. The bottom topography is uniform in the alongshore direction and is the same as that in a previous section, i.e., constant shelf slope with the 100 km offshore width. A rectangular coordinate system on an f-plane is used with x alongshore, y offshore and z vertically upward. We obtain the governing equations without forcing term as follows;

$$\frac{\partial u}{\partial t}+u\frac{\partial u}{\partial x}+v\frac{\partial u}{\partial y}-fv=-g\frac{\partial \eta}{\partial x}+A_h\Delta u-\frac{r_b^2 u\sqrt{u^2+v^2}}{h+\eta} \quad (22)$$

$$\frac{\partial v}{\partial t}+u\frac{\partial v}{\partial x}+v\frac{\partial v}{\partial y}+fu=-g\frac{\partial \eta}{\partial y}+A_h\Delta v-\frac{r_b^2 v\sqrt{u^2+v^2}}{h+\eta} \quad (23)$$

$$\frac{\partial \eta}{\partial t}+\frac{\partial (hu)}{\partial x}+\frac{\partial (hv)}{\partial y}=0 \quad (24)$$

Here, signs of u, v, η, h, f and g are the same as those in the previous section. A_h ($=10^6$ cm^{2}s^{-1}) is the coefficient of lateral eddy viscosity, Δ is the Laplacian operator, r_b^2 ($=2.6\times10^{-3}$) is the quadratic bottom drag coefficient. Equations (22) to (24) are solved numerically using the following boundary conditions. The coast drawn by the thick solid line in Fig. 4 has a slip boundary. At the entrance, η, u and v are prescribed as the driving force. Another conditions at open boundaries are given by the following radiation conditions. At the opposite side boundary against the entrance;

$$\frac{\partial \eta}{\partial t}=\sqrt{gh}\frac{\partial \eta}{\partial x},\ \frac{\partial u}{\partial x}=0,\ v=0 \quad (15).$$

At the offshore boundary;

$$\frac{\partial \eta}{\partial t}=\sqrt{gH0}\frac{\partial \eta}{\partial y},\ \frac{\partial v}{\partial y}=0,\ u=0 \quad (16).$$

The grid size is 20 km$\times$20 km and the time interval is 200 seconds.

We carried out some experiments to confirm the steady barotropic flow solutions obtained in the previous section and to investigate the flow conditions, i.e., inflow and outflow, and its positions against the shelf slope regions. The entrance width ($=50$ km) and the volume transport of the driving force ($=1$ Sv) are the same as those in the previous section. They are fixed in all experiments. The external conditions of five cases are shown in Table 1.

Table 1 Five experiments carried out in the present study

Case	Bottom drag coefficient	Flow conditions at the entrance or exit	Entrance or exit position (x-axis)
1	0	Inflow	0 km
2	2.6×10^{-3}	Inflow	0 km
3	2.6×10^{-3}	Outflow	0 km
4	2.6×10^{-3}	Inflow	600 km
5	2.6×10^{-3}	Outflow	600 km

The ocean is initially at rest. At first, the inflow or outflow transport is increased exponentially up to 1 Sv during 10 days in order to avoid the numerical divergent for the solutions. Then, we observe the steady state spatial distributions of η, u and v. Its steady state flow pattern is reached satisfactorily at 50 days after the start of inflow or outflow in all cases.

Results

Figure 5 shows the steady state spatial distribution of η, u and v without (Case 1) and with (Case 2) the bottom friction, respectively. Although the flow over the shelf slope is dominant in both cases, the alongshore velocity u decreases to the downstream due to the lateral eddy viscosity for Case 1 and bottom friction for Case 2. At the outer shelf region, the onshore flow exists in Case 1 and, on the other hand, the offshore flow in Case 2. Yoon (1982) used the barotropic model in which there is the bottom topography corresponds to Case 1 without the bottom friction and showed that lateral eddy viscos-

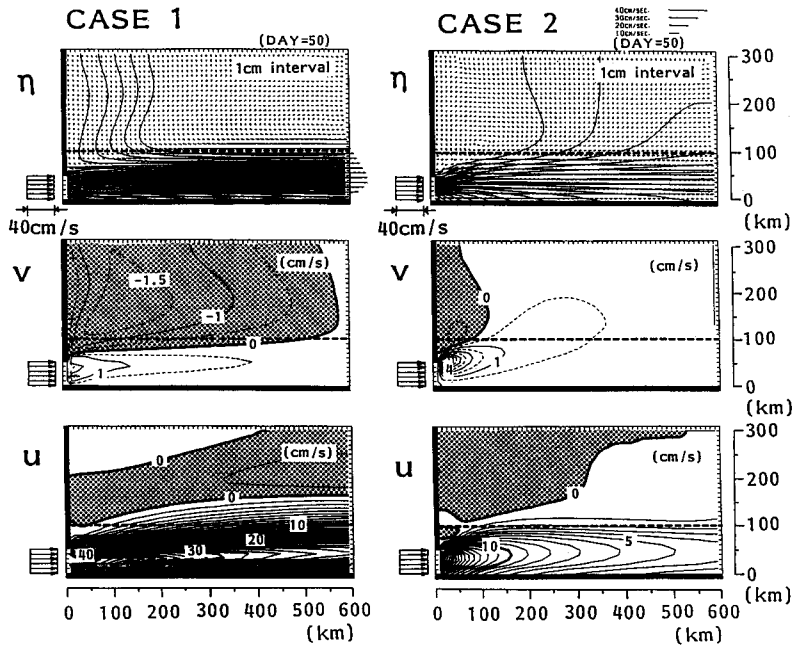

Fig. 5 Horizontal distributions of sea level η and velocity vector (top), offshore velocity v (middle) and alongshore velocity u (bottom) in Cases 1 and 2, given by the numerical experiment. The negative velocity region is shaded.

ity seems to an important factor in determining the flow over the shelf slope. The flow patterns of Case 2 are very similar to those of analytic solution shown in Fig. 3. By comparing Case 1 and Case 2, it is found that the bottom friction remarkably changes the vorticity balance of the barotropic flow over the shelf slope and affects its flow pattern and structure.

Figure 6 shows the spatial distributions of η and the velocity vector in Case 3, 4 and 5. In Case 3 with the outflow exit, the flow has the opposite flow directions to those in Case 2, but its spatial distributions of η and velocity vector are similar to those in Case 2. In this case, the alongshore flow is formed near the exit with the onshore flow, i.e., $v<0$. On the other hand, the alongshore flow over the shelf slope cannot be formed in Cases 4 and 5, although the driving force is induced on the shelf slope. In other words, the bottom controlled flow due to the conservation of the potential vorticity cannot be formed. The strong gradient of η is formed at the entrance or exit and the onshore or offshore flow is dominant there in each case.

The property of the common flow pattern in all cases is that the barotropic flow is formed along on sidewall, that is, the right sidewall to the inflow entrance or the left sidewall to the outflow exit. Such steady flow is formed after the waves are generated during the transient period like as the geostrophic adjustment. As the possible waves in this model, Kelvin wave and topographic Rossby wave are considered. These waves are generated at the source of disturbance, i.e., the entrance or exit, and propagate along the wall to right hand side

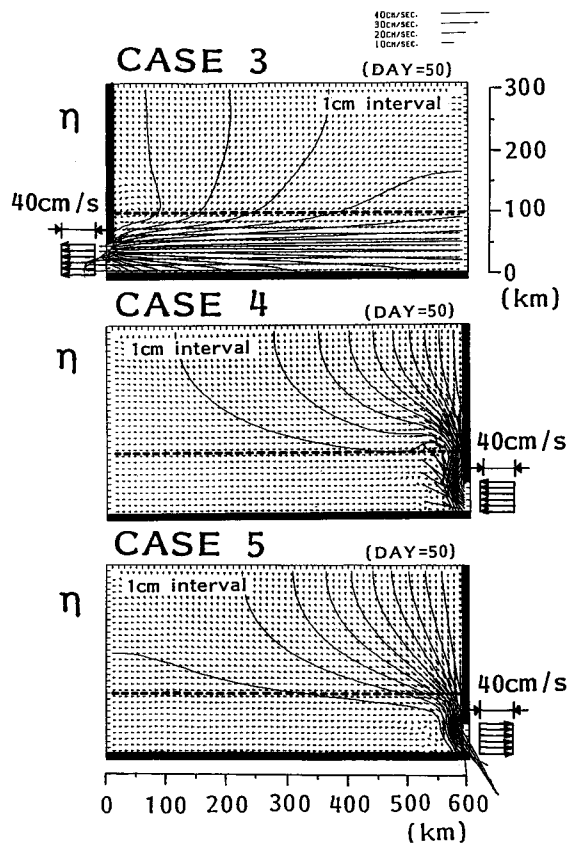

Fig. 6 Horizontal distributions of sea level η and velocity vector in Cases 3, 4 and 5, given by the numerical experiment. The negative velocity region is shaded.

in the northern hemisphere. In result, the steady barotropic flow is formed in the direction of the wave propagation. Yoon (1982) and Kawabe (1982) showed that the topographic wave, i.e., continental shelf wave, contributed to the determination of the steady flow path on the shelf slope. Thus the steady barotoropic flow is related to the coastal trapped wave propagation and may be formed at the right sidewall to source of disturbance in the northern hemisphere regardless the existence of the shelf slope. Therefore, it may be considered that the steady flow in Cases 4 and 5 cannot be formed over the shelf slope which region is opposite side to the direction of the wave propagation.

Applications to the ideal topography around the Tsushima/Korea Strait

In this section, the flow patterns around the Tsushima/Korea Strait in winter will be reproduced in the barotropic model where the ideal topography in taken into account, as shown in Fig. 7(a). In winter the wind driven current due to the strong northwestly wind is prominent in this model area. However, the flow system of this model is only driven by the sea level difference between the East China Sea and the Japan Sea, between we want to understand the dynamics of flow around the Tsushima/Korea Strait and to investigate on how far the influence of its driving force extends in the East China Sea.

The governing equations and some parameters of this model are the same as the previous numerical model. The open boundary conditions of this model are assumed as follows. At the southern end boundary in the East China Sea

$$\eta = 10\ \mathrm{cm},\ \frac{\partial u}{\partial y} = 0,\ v = 0 \qquad (27)$$

At the eastern end boundary in the Japan Sea

$$\int_l \eta(l)dl = 0\ \mathrm{cm},\ \frac{\partial u}{\partial x} = 0,\ \frac{\partial v}{\partial y} = 0 \qquad (28)$$

That is, we suppose that the mean sea level difference of 10 cm between the both open boundaries is maintained. Time interval is 120 seconds.

Figures 7(b) and (c) show the steady state (50 days) spatial distribution of η, velocity vector and absolute value of velocity. In the East China Sea, the strong northward flow is formed along the bottom contour lines more than 50 m depth, and two branches exist in the central part of the East China Sea. One eastward branch inflows into the Tsushima/Korea Strait directly and the other northward branch is the bottom controlled flow. The latter volume transport gradually decreases

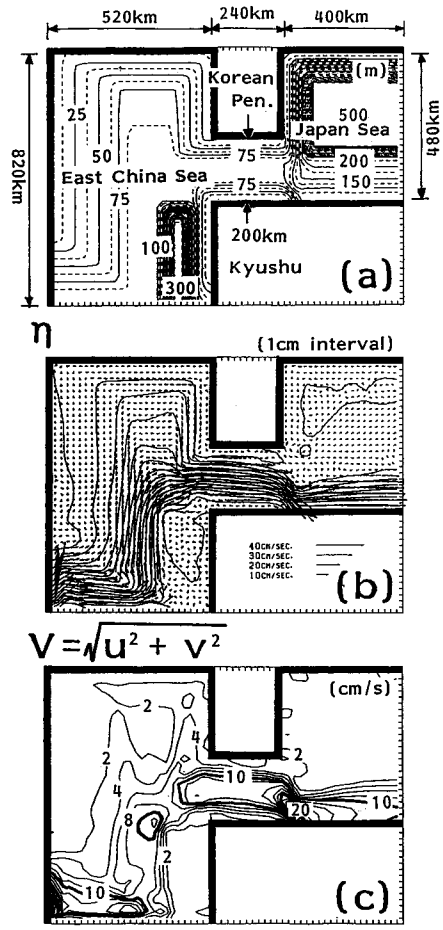

Fig. 7 (a) Schematic view of the model ocean around the Tsushima/Korea Strait. Horizontal distributions of sea level η and velocity vector (b) and the absolute velocity (c) after 50 days.

northward and continues to the southward flow along the west coast of the Korean Peninsula. Consequently, the weak clockwise flow is formed at the northern part of the East China Sea. The southward flow along the west coast of the Korean Peninsula may be generated by the driving force in the Tsushima/Korea Strait like as Case 5 in Fig. 6. On the other hand, the northward flow along the west coast of Kyushu is not formed like as Case 3 in Fig. 6. In spite of neglecting wind stress, two branches simulated by this model are suggested by the observed spatial distributions of surface temperature and salinity in winter shown in Fig. 8, after JODC (1975). Figure 8 shows that the open ocean warm water with salinity more than 34 psu occupies the southern regions in the East China Sea and two branches of this warm water exist near the Cheju Island.

Supposing the effect of the bottom friction varnishes, two branches in the central part of the East China Sea shown in Fig. 7 cannot be generated. Only clockwise flow along isobaths in the northern part of the

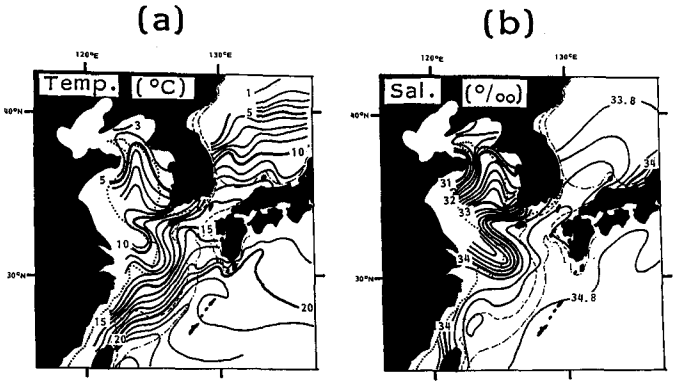

Fig. 8 The mean surface temperature (a) and salinity (b) fields around the Tsushima/Korea Strait after JODC (1975).

East China Sea will be dominant in this case like as Case 1 in Fig. 5, in which the bottom controlled flow is formed remarkably. That is, the flow pattern in Fig. 7 shows that the effect of the bottom friction has weaken the clockwise flow due to the offshore volume transport along the east coast of China. Therefore, the offshore gradient of sea level along the isobaths in the northern part of the East China Sea becomes small, comparing with the case without the bottom friction. Then, the insufficient sea level difference between both sea areas is compensated near the Tsushima/Korea Strait and the eastward branch which inflows directly into the Tsushima/Korea Strait can be formed. An importance of such bottom friction in the East China Sea was also pointed out in Ichiye and Li (1984) by the numerical study. They showed that bottom friction term was about ten percent of the Coriolis term and the nonlinear terms might be less important than the friction term around the Tsushima/Korea Strait.

Conclusion

We investigated the formation and structure of the steady barotropic flow on the shallow shelf slope, using the linear theory and the numerical experiments. The main results of this study are as follows.

(1) The steady barotropic flow over the shallow shelf slope is formed under the balance between the bottom stress curl and vortex stretching of water column on the shelf slope. Thus, the flow over the shelf slope cannot conserve its volume transport.

(2) The maximum alongshore velocity exists at the center of the shelf slope, as distance from the entrance increases.

(3) The steady barotropic flow can be formed in the direction of the coastal trapped wave propagation during the transient period like as the geostrophic adjustment. Thus, in the northern hemisphere the barotropic flow is formed at the right sidewall to the source of disturbance, i.e., entrance or exit. Therefore, the existence of the shelf slope and bottom friction does not play an important role in its formation.

(4) By using the model in which the ideal topography around the Tsushima/Korea Strait is taken into account and the flow system is driven by the sea level difference, two branches of northward branch and eastward branch in the central part of the East China Sea can be simulated. One northward branch is the clockwise flow along isobaths in the northern part of the East China Sea, however its flow is weaken by the bottom friction and offshore gradient of sea level along the isobaths becomes small. Therefore, the other eastward branch near the Tsushima/Korea Strait is formed in order to compensate the insufficient sea level difference between both sea areas.

Acknowledgments

The author expresses his sincere thanks to Prof. Yanagi of Kyushu University for encouragement and to Prof.Takeoka of Ehime University for his helpful discussion. Unfortunately, although the Journal of Oceanography (JO) rejected this paper in 1989, I appreciated the editor and reviewers of JO for critical comments and suggestions. The numerical experiment was carried out on a FACOM N-360 AP of the Computer Center of Ehime University and on a FACOM VP-100 of the Computer Center of Kyushu University.

References

Canady, G.T. (1978) The arrested topographic wave. *J. Phys. Oceanogr.*, **8**, 47-62.

Ichiye, T. and L. Li (1984) A numerical study of circulation in a northeastern part of the East China Sea. pp. 187-207, In : Ocean Hydrodynamics of the Japan and East China Seas, ed. By by T. Ichiye. *Elsevier*, **39**.

JODC (1975) Marine Environmental Atlas, Northwestern Pacific Ocean. *Japan Hydrographic Association, Tokyo*

164 pp.

Kawabe, M. (1982) Branching of the Tsushima Current in the Japan Sea. Part 2. Numerical experiment. *J. Oceanogr. Soc. Japan*, **38**, 183–192.

Nitani, H., S. Yshida, J. Okumoto and N. Nakamura (1978) Statistics on the currents in the seas adjacent to Japan. *Report of Hydorographic Res., Tokyo* **14**, 57–91.

Toba, Y., K. Tomizawa, Y. Kurasawa and K. Hanawa (1982) Seasonal and year-to-year variability of the Tsushima-Tsugaru Warm Current system with its possible cause. *Lar mer*, **20**, 41–51.

Yoon, J.H. (1982) Numerical experiment on the circulation in the Japan Sea. Part 3. Mechanism of the nearshore branch of the Tsushima Current, *J. Oceanogr. Soc. Japan*, **38**, 125–130.